Real-Time Implementation of High Performance Control Scheme for Grid-Tied PV System for Power Quality Enhancement Based on MPPC-SVM Optimized by PSO Algorithm

Abdelbasset Krama [1,2,*] , **Laid Zellouma** [1] , **Boualaga Rabhi** [3] , **Shady S. Refaat** [2] **and Mansour Bouzidi** [4]

1   Electrical Engineering Department, LEVRES Laboratory, El -Oued University, El-Oued 39000, Algeria; zellouma13@yahoo.fr
2   Electrical & Computer Engineering Department, Texas A&M University at Qatar, P.O. Box 23874, Education City, 77874 Doha, Qatar; shady.khalil@qatar.tamu.edu
3   Electrical Engineering Department, LMSE Laboratory, Biskra University, Biskra 07000, Algeria; boualaga@yahoo.fr
4   Département de l'Electronique et des Communications, Faculté des Nouvelles Technologies d'Information et Communication, Université Kasdi Merbah, Ouargla 30000, Algeria; bouzidi.m.28@gmail.com
*   Correspondence: krama.ab@gmail.com or krama.abdelbasset@qatar.tamu.edu; Tel.: +21-364-291-514

check for updates

Abstract: This paper proposes a high performance control scheme for a double function grid-tied double-stage PV system. It is based on model predictive power control with space vector modulation. This strategy uses a discrete model of the system based on the time domain to generate the average voltage vector at each sampling period, with the aim of canceling the errors between the estimated active and reactive power values and their references. Also, it imposes a sinusoidal waveform of the current at the grid side, which allows active power filtering without a harmonic currents identification phase. The latter attempts to reduce the size and cost of the system as well as providing better performance. In addition, it can be implemented in a low-cost control platform due to its simplicity. A double-stage PV system is selected due to its flexibility in control, unlike single-stage strategies. Sliding mode control-based particle swarm optimization (PSO) is used to track the maximum power of the PV system. It offers high accuracy and good robustness. Concerning DC bus voltage of the inverter, the anti-windup PI controller is tuned offline using the particle swarm optimization algorithm to deliver optimal performance in DC bus voltage regulation. The overall system has been designed and validated in an experimental prototype; the obtained results in different phases demonstrate the higher performance and the better efficiency of the proposed system in terms of power quality enhancement and PV power injection.

Keywords: shunt active power filter; photovoltaic; sliding mode; PSO; model predictive control

1. Introduction

Nowadays, the use of renewable energies is more than necessary; it is a global strategic issue. Indeed, It is a major tool against global warming [1]. It is crucial to preserve resources and the environment while meeting the global demand for energy [2,3]. Solar energy is one of the so-called renewable energies in the sense that the sun is almost an inexhaustible resource [4].

It appears that photovoltaic presents itself as a solution for the future [5] because it offers a multitude of advantages; photovoltaic energy is exploitable in a mountainous area, in a remote village,

and in the center of a big city [6], because sunlight is available almost everywhere. Photovoltaic electricity can be produced as close as possible to its place of consumption in a decentralized way [7], directly to the user, which makes it accessible to a large part of the world's population.

Much research and development are conducted about the critical elements of photovoltaic energy; starting with energy generation [6], conversion, then injection into the network [8], as well as energy management [9]. The key problem with photovoltaic energy generation is the difficulty of achieving the highest energy yield for PV panels. The voltage of a PV panel strongly depends on the connected load due to the non-linear behavior of the PV cell [10]. Therefore, various Maximum Power Point Tracking (MPPT) algorithms have been established to allow panels operate in optimal conditions, and thus, to track the maximum power point [6,11]. Among these algorithms are "Perturbation & Observation (P&O)" [12] and "incremental conductance (InCon)" [13] which are the most used due to the simplicity of their implementation. However, the abovementioned methods are constrained by the amplitude of the injected perturbations, which determines the importance of the oscillations around the Maximum power point (MPP) as well as the convergence time. To overcome this problem, several algorithms have been developed based on techniques derived from artificial intelligence such as Fuzzy Logic [14], Neural Network [15], Neuro-Fuzzy [16], and Metaheuristic algorithms [17–19]. These approaches allow faster convergence to MPP, and reduce oscillations around this point. Nevertheless, these kinds of algorithms often take huge computation time, which requires a high-speed microprocessor to implement. As a compromise, Sliding mode control (SMC) -based MPPT has been selected [20] due to its accuracy and high robustness in maximum power tracking [21]. It may be an interesting alternative, especially in cases of sudden changes in solar irradiance [22].

On the other hand, the widespread use of nonlinear loads in manufacturing activities as well as for domestic reasons has had an undesirable impact on the quality of electric power systems [23,24]. These nonlinear loads draw non-sinusoidal currents from utility grids, which create harmonic currents and low power factors [25,26]. The latter present many harmful effects like power losses, heat and saturation of transformers, and the degradation of electrical devices [25,27]. On the other hand, the increased demand of good quality of power makes the use of power quality improvement devices essential [28], and much research is interested in double function grid-tied PV systems to simultaneously perform power quality improvement and active power injections.

The control of double function grid-tied PV system is an effective research field, and numerous control strategies have been discussed in the literature [1,24,29–31]. They are mainly classified into two main categories: direct and indirect methods. The direct methods have been extensively reported in the literature [1,4,32]. They are based on direct reference current harmonic extraction, as they determine harmonic components to be canceled by using different algorithms such as instantaneous active and reactive power (p_q theory) [4,33], synchronous reference frame (SRF) [32,34], Second Order Generalized Integrator algorithm (SOGI) [1]. However, the application of such an algorithm needs powerful computation resources that result in a relatively slow response times. Also, the implementation of the aforementioned algorithms requires current sensors on two different sides: at the load, and after the inverter or after the main source. Moreover, it needs two other voltage sensors for the main source and the DC side. Reducing the number of sensors becomes an interesting subject due to many returns such as cost, size reduction, simplicity of implementation, and avoiding precision loss. In recent years, indirect control strategies have aroused the attention of many researchers; such strategies include Direct Power Control (DPC), that focuses on a predefined switching table to select the appropriate control vector [24,35,36], a predictive direct power control (P-DPC) based on cost function minimization, and predictive current control, that uses the currents as control variables instead of powers as in P-DPC [29,37]. These three strategies require current sensors only at the main source; they do not take into consideration the impact of load or filter current compared to conventional ones. However, these control strategies are more effective than conventional ones but still possess undesirable properties such as the accuracy of compensation, power ripples, and variable and high switching frequency, which lead to high power losses and reduce the reliability of power system.

Currently, moving towards approaches that provide fixed switching frequency is a vital issue. In this context, many algorithms that have been designed with fixed switching frequencies have been proposed for grid-connected converters [38–40].

The main contribution of this paper is to propose a high-performance control scheme for double function grid-tied PV system based on model predictive power control (MPPC) with space vector modulation (SVM). This approach is used to solve the variable frequency of MPPC based on cost function minimization that was presented in [23,37]. Moreover, it requires a reduced number of sensors compared to that presented in [1,4]. In addition, it offers a high capability in harmonic current mitigation and power factor correction, as well as in active power injection. In addition, it operates at low switching frequencies [41]. The Particle swarm optimization algorithm (PSO) became one of the most useful and most popular algorithms to solve various optimization problems in various fields. Among the key features of the PSO are its simplicity and flexibility. However, it is a powerful algorithm [42]. The parameters of Linear Proportional-Integral (PI) controller with anti-windup, which is used to perform the control of DC bus voltage, have been tuned through a particle swarm optimization algorithm considering Integral Time Absolute Error (ITAE) as an objective function [43,44]. The performance of the proposed PSO-PI controller has been compared to that of an ordinary PI controller, which is achieved through a computing approach. The gain of sliding mode MPPT has been tuned offline using the PSO algorithm to find the optimum gain that provides good accuracy in tracking the MPP. The efficiency and the performance of the proposed system have been investigated using real-time hardware implementation based on dSPACE board (dS1104). The obtained results in various cases (at filter switch on, load variation, after connecting PV system) present good static performance as compared to the DPC approach, whereas the dynamic performance has been improved after using anti-windup PI controller optimized by the PSO algorithm.

The paper is structured as follows: In Section 1, a comprehensive overview is presented. The general configuration of the global system is described in Section 2. Section 3 explains the basic principle of the proposed control strategy based on the MPPC-SVM approach, and presents its mathematical model. In Section 4, modeling and control of PV system are presented. After that, Section 5 takes a look at the particle swarm optimization algorithm and the optimization of different parameters. Then, in Section 6, the experimental results are given with a discussion. Lastly, the conclusion is given in Section 7.

2. General Configuration of the System

The proposed system relies on four main parts, as depicted in Figure 1: the power supply, nonlinear load, voltage source inverter (VSI) and double stage PV system. The inverter has a double function. Firstly, it operates as shunt active filter by minimizing the current harmonic distortion of the grid and suppressing the phase shift that are caused by the nonlinear load. Then, it injects PV power into the load/grid. PV panels are connected to VSI via a boost converter to operate with MPPT. The three-phase network is connected to a nonlinear load via three inductors. The nonlinear load is shaped from a three-phase diode rectifier with a resistive load, which is the most common source of harmonic currents. A two-level VSI based on six IGBT switches with a capacitor for energy storage is connected at the point of common coupling (PCC) through the inductors (L_f).

The instantaneous voltage of the three-phase balanced and sinusoidal system is based on the following expression:

$$v_{sa}(t) = \sqrt{2}v_s \cos(\omega t)$$
$$v_{sb}(t) = \sqrt{2}v_s \cos(\omega t - 2\tfrac{\pi}{3})$$
$$v_{sc}(t) = \sqrt{2}v_s \cos(\omega t + 2\tfrac{\pi}{3})$$

(1)

The measured voltages at PCC are passed through the phase-locked loop (PLL) to estimate the fundamental component of the supply voltage. The theoretical principle of PLL is discussed in [45].
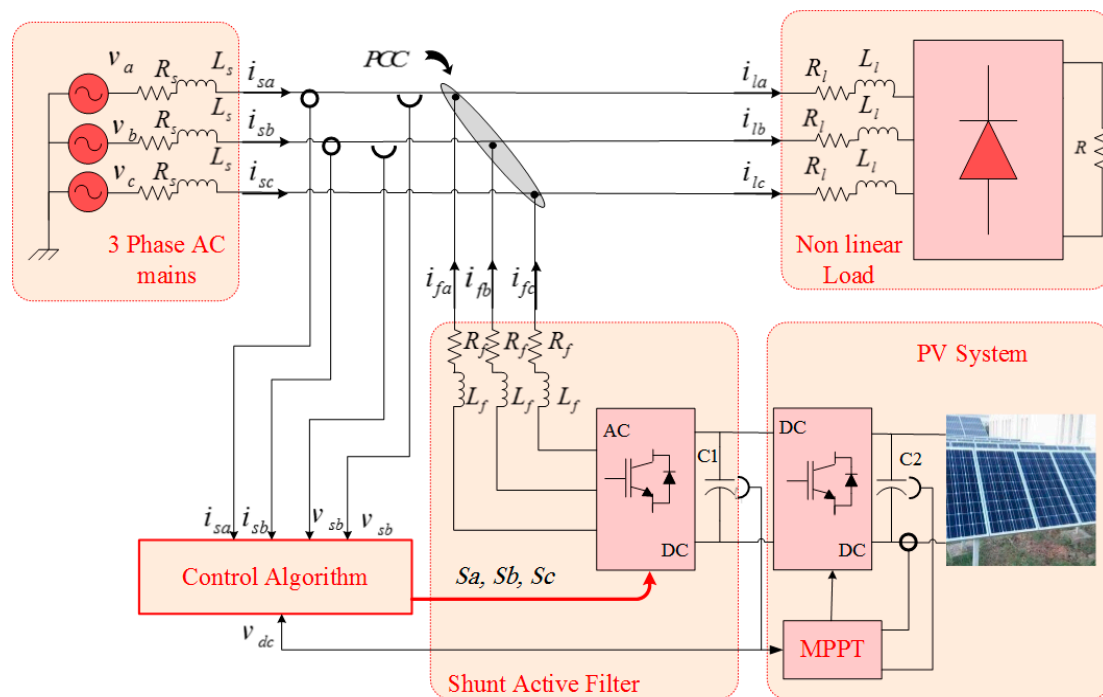
Figure 1. General configuration of the proposed system.

The equation that connects the current and the voltage of the active filter will be obtained after the application of Kirchhoff's laws to the above circuit, and can be expressed as follows:

$$L_f \frac{di_{fx}}{dt} + R_f i_{fx} = u_{fx} - v_{sx}, \; x = a, b, c \tag{2}$$

where v_s is the source voltage at PCC, and u_f is the voltage at the output of the inverter.

By neglecting the effect of filter resistance, Equation (2) can be written as:

$$L_f \frac{di_{fx}}{dt} = u_{fx} - v_{sx} \tag{3}$$

where:

$$v_{sx} = v_x - L_s \frac{di_{sx}}{dt} + R_s \cdot i_{sx} \tag{4}$$

where: v_s is the measured voltage at PCC, v is the source voltage, and i_s is the source current.

The basic topology of the two-level VSI, as displayed in Figure 1, comprises six switches. Such a structure makes it possible to make eight combinations of switching that provide eight voltage vectors at the output of the inverter. Two voltages vectors are null and the others are given by expression (5).

$$u_n = \begin{cases} \frac{2}{3} v_{dc} e^{j(n-1)\frac{\pi}{3}} & n = 1...6 \\ 0 & n = 0,7 \end{cases} \tag{5}$$

where v_{dc} is the DC bus voltage, n is a number of voltage vector, and u_n is the value of voltage vector at the output of VSI.

3. Control Structure

3.1. General Description of MPPC-SVM Approach

The MPPC-SVM strategy, as illustrated in Figure 2, relies on forecasting the instantaneous active and reactive power values using a predictive model. The control of VSI uses the concept of applying an average voltage vector, in each sampling period, that is converted into a sequence of adjacent control vectors in order to obtain the desired active and reactive powers [38]. The predictive value of active power is calculated by the outer control loop of the DC bus voltage based on a predictive model. The reactive power value is almost zero to ensure power factor correction. The optimal parameters of the anti-windup PI controller are calculated offline using PSO that takes into consideration total harmonic distortion of supply current $THD(t)$ and the error of the DC bus voltage control loop as an objective function. A detailed description of this model is provided below.
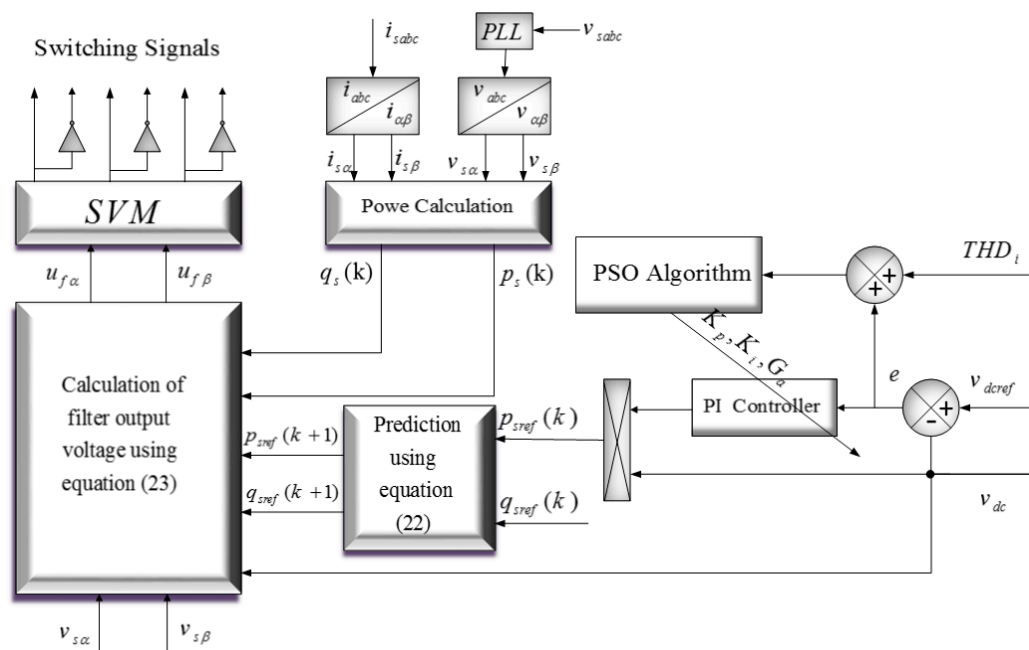

Figure 2. Block diagram of MPPC-SVM approach.

3.2. Computational Analysis of the Model

Any predictive strategy is based mainly on predicting the control quantities to be applied during a sampling period in order to accomplish the favorite performance. Firstly, the variable quantities that will be controlled in the proposed predictive model are the active and reactive powers. The balanced three-phase system, and the active and reactive power expressions in a stationary reference frame (α, β) are defined as:

$$\begin{bmatrix} p_s \\ q_s \end{bmatrix} = \begin{bmatrix} v_{s\alpha} & v_{s\beta} \\ v_{s\beta} & -v_{s\alpha} \end{bmatrix} \begin{bmatrix} i_{s\alpha} \\ i_{s\beta} \end{bmatrix} \tag{6}$$

The variation of instantaneous active and reactive powers can be obtained using the time derivative as follows:

$$\frac{d}{dt}\begin{bmatrix} p_s \\ q_s \end{bmatrix} = \frac{d}{dt}\begin{bmatrix} v_{s\alpha} & v_{s\beta} \\ v_{s\beta} & -v_{s\alpha} \end{bmatrix} \begin{bmatrix} i_{s\alpha} \\ i_{s\beta} \end{bmatrix} + \begin{bmatrix} v_{s\alpha} & v_{s\beta} \\ v_{s\beta} & -v_{s\alpha} \end{bmatrix} \frac{d}{dt}\begin{bmatrix} i_{s\alpha} \\ i_{s\beta} \end{bmatrix} \tag{7}$$

If the sampling period is infinitely small compared with the fundamental period, the discretization of the Equation (7) yield:

$$\begin{bmatrix} p_s(k+1) - p_s(k) \\ q_s(k+1) - q_s(k) \end{bmatrix} = \begin{bmatrix} v_{s\alpha} & v_{s\beta} \\ v_{s\beta} & -v_{s\alpha} \end{bmatrix} \begin{bmatrix} i_{s\alpha}(k+1) - i_{s\alpha}(k) \\ i_{s\beta}(k+1) - i_{s\beta}(k) \end{bmatrix} \tag{8}$$

In SAPF, the load consumes non-sinusoidal current that is composed mainly of the source current in addition to the current generated by the filter. The fundamental current is ensured by the source and the filter provides the harmonic currents as detailed below.

$$i_{lx} = i_{sx} + i_{fx}, \ x = a, b, c \tag{9}$$

$$i_{lx} = i_{\text{fundamental x}} + i_{harmonic \ x} \tag{10}$$

$$i_{fx} - i_{harmonic \ x} = i_{\text{fundamental x}} - i_{sx} \tag{11}$$

where:

i_l: Current consumed by the load.

i_f: Current generated by the filter.

$i_{fundamental}$: Fundamental component of the current.

$i_{harmonic}$: Harmonic components of the current.

It can be noticed that the variation in filter current is equal to that of source current but with opposite sign:

$$i_{fx} - i_{harmonic \ x} = -(i_{sx} - i_{fundamental \ x}) \tag{12}$$

Then

$$\Delta i_{fx} = -\Delta i_{sx} \tag{13}$$

For a small variation of source and filter currents, the Equation (13) can be written as:

$$di_{fx} = -di_{sx} \tag{14}$$

The last expression allows us to obtain the variation in filter current as well as the voltage at the point of common coupling PCC without the need to measure filter current. Thus, the Equation (3) will be:

$$L_f \frac{di_{sx}}{dt} = v_{sx} - u_{fx}, \ x = a, b, c \tag{15}$$

The variation of the source current in α-β reference frame is given by the following expression:

$$\begin{bmatrix} i_{s\alpha}(k+1) - i_{s\alpha}(k) \\ i_{s\beta}(k+1) - i_{s\beta}(k) \end{bmatrix} = \frac{T_s}{L_f} \left(\begin{bmatrix} v_{s\alpha}(k) \\ v_{s\beta}(k) \end{bmatrix} - \begin{bmatrix} u_{f\alpha}(k) \\ u_{f\beta}(k) \end{bmatrix} \right) \tag{16}$$

By inserting the previous expression into Equation (8), the predictive values of active and reactive power can be obtained by the following predictive model:

$$\begin{bmatrix} p_s(k+1) - p_s(k) \\ q_s(k+1) - q_s(k) \end{bmatrix} = \frac{T_s}{L_f} \begin{bmatrix} v_{s\alpha}(k) & v_{s\beta}(k) \\ v_{s\beta}(k) & -v_{s\alpha}(k) \end{bmatrix} \left(\begin{bmatrix} v_{s\alpha}(k) \\ v_{s\beta}(k) \end{bmatrix} - \begin{bmatrix} u_{f\alpha}(k) \\ u_{f\beta}(k) \end{bmatrix} \right) \tag{17}$$

It is observed that the sampling period, as well as filter and source inductance, are the main parameters that play an important role in the prediction stage.

The objective of the predictive algorithm consists of tracking the active and reactive power values by making the error between the reference value and the actual value as near to zero as possible:

$$\begin{cases} \varepsilon_p(k) = p_{sref}(k) - p_s(k) \approx 0 \\ \varepsilon_q(k) = q_{sref}(k) - q_s(k) \approx 0 \end{cases} \tag{18}$$

For an optimal convergence towards the desired values of powers, the following equations must be verified.

$$\begin{cases} p_s(k+1) - P_{sref}(k+1) = 0 \\ q_s(k+1) - q_{sref}(k+1) = 0 \end{cases} \tag{19}$$

Then

$$\begin{cases} p_s(k+1) = p_{sref}(k+1) \\ q_s(k+1) = q_{sref}(k+1) \end{cases} \tag{20}$$

By inserting the Equation (20) into (17):

$$\begin{bmatrix} p_{sref}(k+1) - p_s(k) \\ q_{sref}(k+1) - q_s(k) \end{bmatrix} = \frac{T_s}{L_f} \begin{bmatrix} v_{s\alpha}(k) & v_{s\beta}(k) \\ v_{s\beta}(k) & -v_{s\alpha}(k) \end{bmatrix} \left(\begin{bmatrix} v_{s\alpha}(k) \\ v_{s\beta}(k) \end{bmatrix} - \begin{bmatrix} u_{f\alpha}(k) \\ u_{f\beta}(k) \end{bmatrix} \right) \tag{21}$$

By considering this, the reference value of active power is varied linearly between two successive sampling periods, as described in Figure 3. This consideration makes the assumption that the variation of the error of the voltage regulation loop during two successive sampling periods is null.
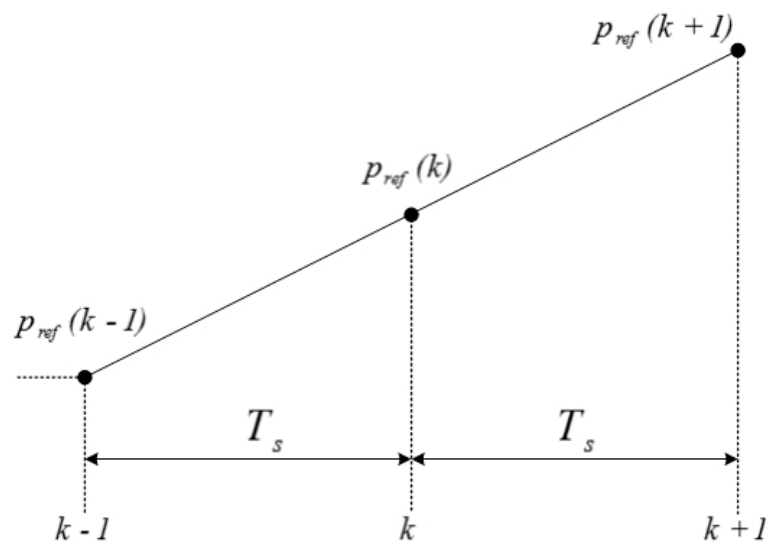

Figure 3. Predictive value estimation of reference active power.

In contrast, the reference value of reactive power is often imposed as a constant with zero value in order to ensure an operation with the unity power factor. As a result, the reference values of active and reactive power for the next sampling period can be estimated by the following:

$$\begin{bmatrix} p_{sref}(k+1) \\ q_{sref}(k+1) \end{bmatrix} = \begin{bmatrix} 2p_{sref}(k) - p_{sref}(k-1) \\ q_{sref}(k) \end{bmatrix} \tag{22}$$

By using the Equations (21) and (22), the average control vector to be applied during the sampling period $[kT_s\ (k+1)T_s]$ is obtained by the following equation:

$$\begin{bmatrix} u_{f\alpha}(k) \\ u_{f\beta}(k) \end{bmatrix} = \begin{bmatrix} v_{s\alpha}(k) \\ v_{s\beta}(k) \end{bmatrix} - \frac{L_f}{T_s(v_{s\alpha}{}^2+v_{s\beta}{}^2)} \begin{bmatrix} v_{s\alpha}(k) & v_{s\beta}(k) \\ v_{s\beta}(k) & -v_{s\alpha}(k) \end{bmatrix} \begin{bmatrix} 2p_{sref}(k) - p_{sref}(k-1) - p_s(k) \\ q_{sref}(k) - q_s(k) \end{bmatrix} \quad (23)$$

3.3. Control of DC Bus Voltage

The control of the DC bus voltage of VSI is an essential stage to ensure a good operation of the whole system. A DC side control loop is necessary to make the voltage constant and to estimate the reference value of grid current. A proportional integral controller (PI) has been proposed to correct the oscillation of the DC bus voltage and to ensure the stability of the system. Hence, the gains of the PI controller are computed as [35]:

$$k_P = 2 \cdot \xi \cdot C_1 \cdot \omega_n \quad (24)$$

$$k_i = \omega_n^2 \cdot C_1 \quad (25)$$

where ω represents the natural frequency, whereas ξ is the frequency of damping which is equal to 0.707 for optimal operation.

In spite of this, high performance cannot be achieved by PI controller, in transient time, because of the large error that is caused by the saturation of controller [46]. A high gain of anti-windup has been introduced to the PI controller (G_a), as depicted in Figure 4 [35,46], with the aim of solving saturation problem and obtaining smooth operations in the transient state.
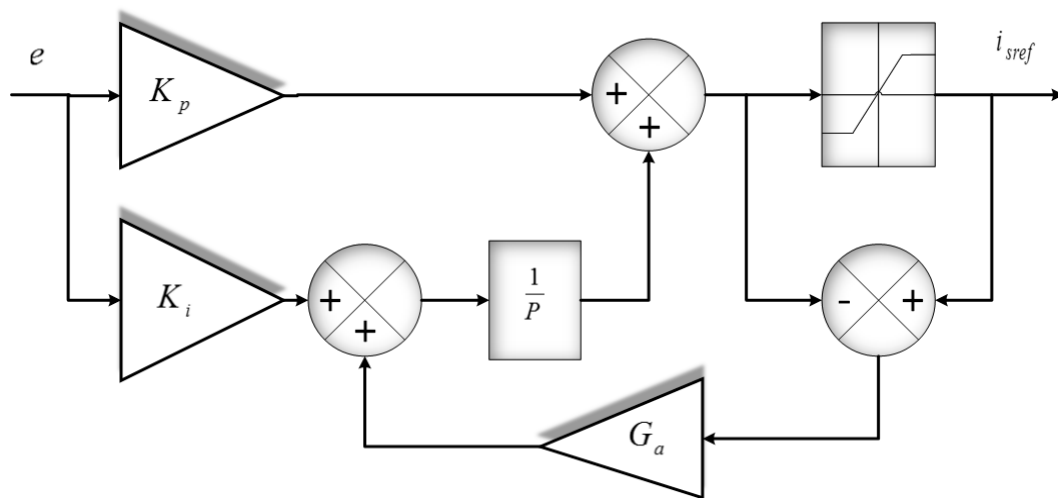

Figure 4. Block diagram of proportional integral controller joined with anti-windup gain.

4. Photovoltaic System

4.1. Modeling of Solar PV Module

PV module is treated as a number of PV cells associated in series and in parallel [47]. Multiple mathematical models for PV cells are found in the literature [48,49]. The adopted PV module is designed based on a single-diode model represented by Equation (26) [49].

$$I_{pv} = I_{sc} - I_0 \cdot [\exp(\frac{V_{cell} + R_s \cdot I_{cell}}{V_t \cdot \alpha}) - 1] - \frac{V + R_s \cdot I_{cell}}{R_p} \quad (26)$$

where:

I_{sc}: Photo-current generated by PV cell.

I_0: Saturation current of the diode.

V_t: Thermal voltage of PV cell.

R_p: The equivalent parallel resistance.

Rs: The equivalent series resistance.

α: Diode ideality factor.

V_{cell}: Voltage at the output of PV cell.

I_{cell}: Current generated by PV cell.

In the experiment, four PV modules (ALPV85-125M-36) are connected in series to achieve the desired voltage level and to raise the power of the whole PV system. However, the installation of the PV modules depends on its geographical location. It is necessary to choose the optimal orientation and inclination for the location. This makes it possible to produce a maximum of energy. The PV modules are oriented south (azimuth 0°) and inclined 34.8° relative to the horizontal, which is the optimum tilt angle in that location, as demonstrated in [50]. The parameters of the PV panel are listed in Table 1, whereas the P-V and I-V characteristics of the overall PV system in different climate conditions are given in Figure 5.

Table 1. The main parameters of the proposed PV module.

Parameters of the PV Module ALPV85-125M-36	
Maximum power Pmax	85 W (±5%)
Maximum power point Voltage (Vmpp)	17.36 V
Open circuit voltage (Uoc)	22.38 V
Maximum power point Current (Impp)	4.95 A
Short circuit current (Ioc)	5.48 A
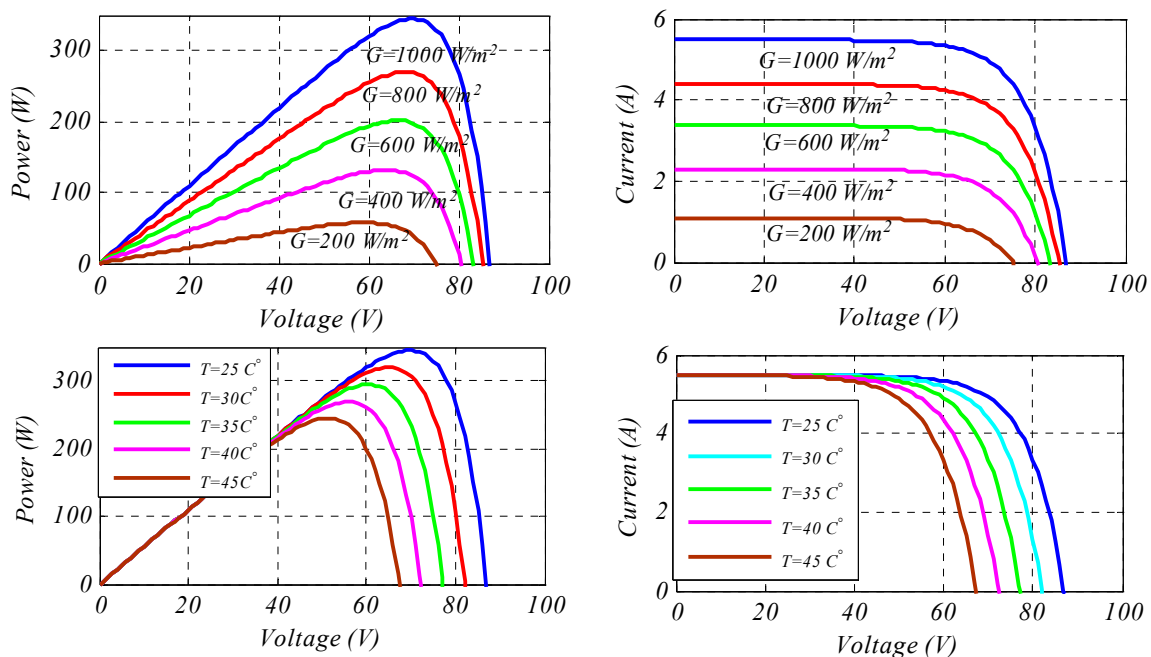
Figure 5. P-V and I-V characteristics of the overall PV system.

4.2. Sliding Mode Based MPPT

Sliding mode control for non-linear systems has become a motivating solution. It is one of the most used control approaches thanks to its advantages.(robustness, good stability, and very low response time) [51]. It is characterized by the discontinuity of the control at the passages by a sliding

surface. So everything depends on the appropriate choice of this surface [20]. Therefore, for simplicity, Equation (27) has been transformed for the sliding surface for SM-MPPT.

$$S = \frac{dP_{pv}}{dI_{pv}} \tag{27}$$

Then

$$S = I_{pv}\frac{dV_{pv}}{dI_{pv}} + V_{pv} \tag{28}$$

The structure of the sliding mode controller focuses on two main parts: a continuous part and another discontinuous part [51], as presented below:

$$u = u_{con} + u_{disc} \tag{29}$$

The first part, is extracted from the condition (30) which satisfies Lyapunov stability theory [52].

$$d\dot{S} = 0 \tag{30}$$

The continuous part is as follows (31).

$$u_{con} = 1 - \frac{V_{pv}}{V_{dc}} \tag{31}$$

The second part is important in nonlinear control because its role is to eliminate the effects of inaccuracies and disturbances on the model of the system when the system has not reached the sliding surface [20]. It is defined by:

$$u_{disc} = K{\cdot}sign(S) \tag{32}$$

K: is the maximum value desired at the output of the controller to assure steady-state stabilization. The output of the SMC can be represented by (33):

$$u = \begin{vmatrix} 1 & if & (u_{con} + u_{disc}) > 1 \\ (u_{con} + u_{disc}) & if & 0 < (u_{con} + u_{disc}) < 1 \\ 0 & if & (u_{con} + u_{disc}) < 0 \end{vmatrix} \tag{33}$$

The sliding mode gain has been tuned using PSO algorithm as shown in Figure 6.
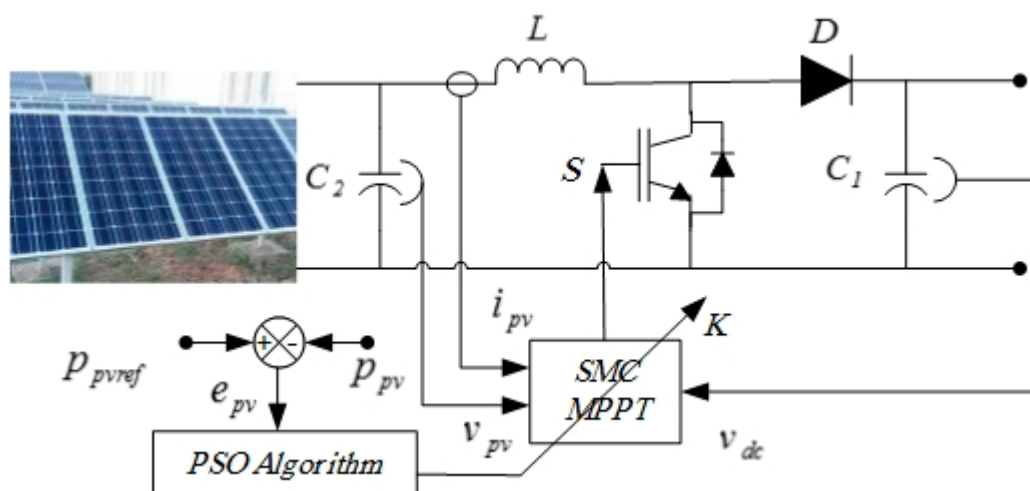

Figure 6. Control of PV system using sliding mode MPPT based PSO.

5. Parameters Optimization Using PSO

5.1. Designing of PSO Algorithm

PSO contains a population of candidate solutions called a swarm; this swarm is a set of particles [44]. Any particle has a position in the search space y. Therefore, any particle has a velocity h, which describes the movement of a particle in the sense of direction, distance, and the step size. In addition to position and velocity, every particle has a memory of its own best position and best experience. This is denoted by the personal best P_{best}. However, the best experience of all particles is known as the global best G_{best} [53]. Particles of the swarm are interacting and learning from each other, obeying some simple rules to find the best solution for an optimization problem [54]. The mathematical model of the motion of particles can be described as follows:

$$h_i(k+1) = \delta(k)h_i(k) + r_1 o_1(P_{best(i)}(k) - y_i(k)) + r_2 o_2(G_{best(i)}(k) - y_i(k)) \tag{34}$$

$$y_i(k+1) = y_i(k) + h_i(k+1) \tag{35}$$

where:

i: Number of particle.

k: Current number of iteration.

r_1, r_2: are random number confined between 0 and 1.

o_1, o_2: are acceleration coefficients.

δ: is the inertia coefficient that is defined by (36) as indicated in [55].

$$\delta(k) = \delta_{\max} - \left(\frac{\delta_{\max} - \delta_{\min}}{\delta_{\max}}\right) \cdot k \tag{36}$$

The new position of a particle is probably a better location, because it is created according to the previous decision about the movement of this particle, and it uses the previous experience of the particle itself as well as the previous experience of the whole swarm.

5.2. The Optimization Problem

A PI controller with anti-windup provides good performance in DC bus voltage regulation for the proposed system. However, anti-windup PI controller needs an accurate mathematical model, which is unreachable in the case of parameter variations and system nonlinearity. Consequently, a PI controller that is designed based on the conventional method fails to achieve optimal performance under different operating modes. Hence, the PSO algorithm has been proposed to improve the performance of the anti-windup PI controller. It executes an offline search in three search spaces to obtain the optimized parameters for the PI controller, i.e., integral gain *Ki*, proportional gain *Kp*, and anti-windup gain *Ga* that give better dynamic and steady performance.

The optimization problem, which is being solved by the PSO, is an objective function that would like to minimize its fitness. The objective function is based on the instantaneous error of DC bus voltage control loop $e(t)$ and instantaneous $THD(t)$ of current supply, as described in Figure 2:

$$ITAE = \int t|J(t)| \cdot dt \tag{37}$$

whereas:

$$J(t) = e(t) + THD_{i_s}(t) \tag{38}$$

The performance of above-mentioned objective functions is evaluated according to the PSO mechanism, as shown in Figure 7; the initial parameters of the PSO algorithm are listed in Table 2. The suitable objective function for DC bus voltage regulation was selected according to its corresponding

fitness value. After many experiments, the lowest fitness value has been obtained using ITAE objective function.

$$ITAE = \int t|e_{pv}(t)|\cdot dt \tag{39}$$

where:

$$e_{PV}(t) = P_{PVref}(t) - P_{PV}(t) \tag{40}$$

where

$P_{PVref}(t)$: Reference value of output PV power.
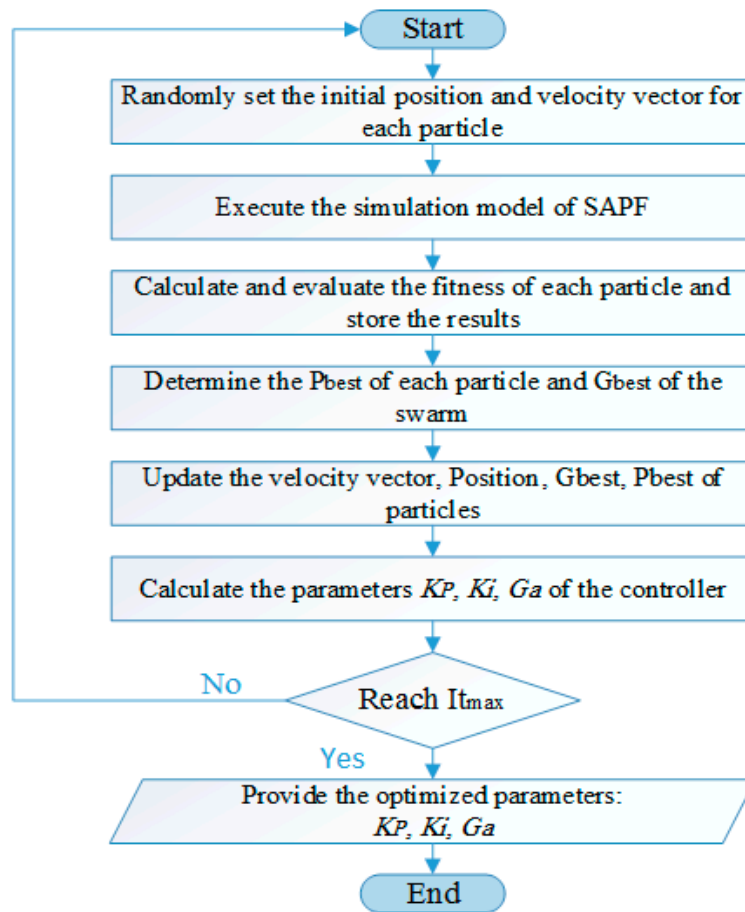$P_{PV}(t)$: Measured value of output PV power.

Figure 7. Flowchart of PSO mechanism.

Table 2. Main parameters of PSO Algorithm.

Number of particles in a swarm	50
Max number of iteration k_{max}	40
Acceleration coefficients o_1, o_2	2
Inertia coefficients $\delta_{min}, \delta_{max}$	0.6, 0.9

Then again, sliding mode gain is properly adjusted for each sliding mode application with the aim of satisfying the stability condition of the system, because there is no generalized rule to determine SMC gain [56]. The PSO algorithm has been used to determine the optimal gain for sliding mode MPPT considering the objective function ITAE in standalone mode. Thus, the obtained optimized and calculated gains are given in Table 3.

Table 3. Optimized and calculated gains.

	Optimized Gains	Calculated Gains
DC bus controller	Kp = 0.176, Ki = 6.714, Ga = 456.17	Kp = 0.1, Ki = 6.12, Ga = 1000 (chosen manually)
SMC gain	K = 0.074	-

6. Results and Discussion

The proposed system has been investigated in an experimental bench test developed in the laboratory, as shown in Figure 8. The experimental pattern is designed for low voltage rates due to laboratory limitations. It consists mainly of the following:

1. Three phase power supply based on three-phase autotransformer.
2. Two-level inverter and boost converter manufactured by SEMIKRON based on IGBTs (SKM 50 GB 123D) in addition to three-phase diode bridge rectifier.
3. Measurement and visualization tools.
4. Coils and resistor load.
5. Four PV Panels (ALPV85-125M-36).
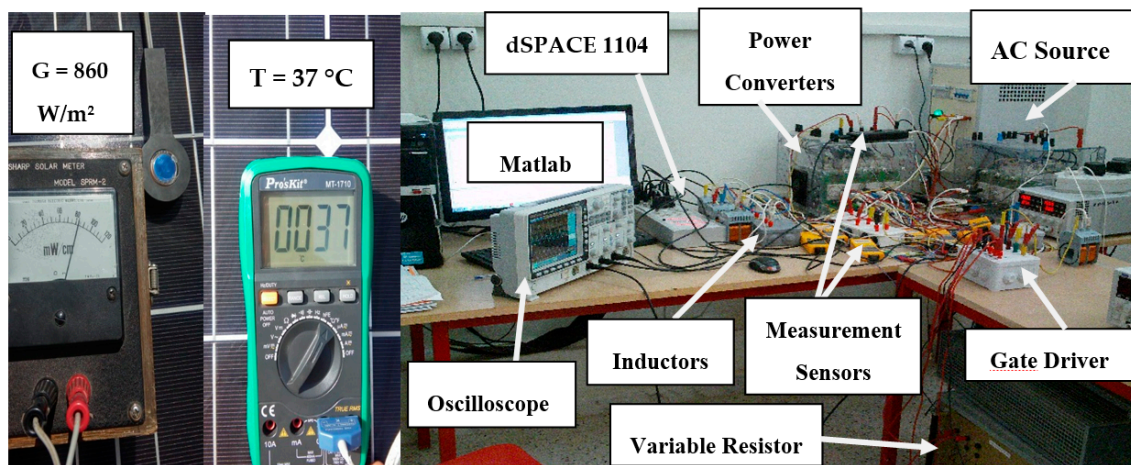
Figure 8. Experimental test bench.

All the experimental results were recorded through a four-channel Oscilloscope Instek GDS-3154, 150 MHz, 5 GSa/s (Giga Samples per Second). The size of memory necessary to stock a captured signal based on two parameters depends on the sample rate and the waveform length (time period). The waveform length is the product of the horizontal scale multiplied by the number of divisions. The used oscilloscope has 10 horizontal divisions and the sample rate as equal to 5 GS/s. The lowest horizontal scale used in the measurement is 10 ms/div. The total time period is 10 div × 10 ms/div. Then, the necessary waveform memory could be calculated as follows: 10 × 10 ms × 5 GS/s = 0.5 GSample (half million sample). On the other hand, the frequency range of the used oscilloscope is 150 MHZ, which designates the bandwidth of an input signal that can be captured with negligible loss. However, the frequencies of the measured signals do not exceed 2 kHz. Therefore, the used oscilloscope (Instek GDS-3154, 150 MHz, 5 GSa/s) can effectively capture the details of the signals with high accuracy.

The thermometer of a digital multimeter Pro'skit MT-1710 was used for measuring the temperature. It is characterized as follows: −20 to 400 °C ± (1.0% + 5 digits)/400 to 1000 °C ± (1.5% + 15 digits). However, it is used to measure temperatures below 400 °C, allowing it to provide higher accuracy ± (1.0% + 5 digits).

The pyranometer SHARP SOLAR METER SPRM-2 was used for measuring solar irradiance. Its irradiance range is 0 to 1200 W/m^2.

For real-time implementation, dSpace 1104 is used. The computing time of the process is set to the lowest possible sample time of the DSP (4×10^{-4} S). The detailed system parameters are given in Table 4.

Table 4. Parameters of power circuit.

Source		Load		SAPF		Boost	
Vs	65 V	Lc	1 mH	Rf	0.9 Ω	L	5 mH
f	50 Hz	Rc	0.6 Ω	Lf	4 mH	C2	560 μF
Rs	0.45 Ω	Rl	11 Ω	C1	1100 μF		
Ls	2.5 mH						

Firstly, the performance of PSO-PI with anti-windup is compared to that of the conventional PI controller. The response of each one under double step change of DC bus voltage from 160 V to 140 V and vice versa is shown in Figure 9. It is noted that PSO-PI with anti-windup can improve the transient state by dipping the over- and upper- shoot of DC-link voltage, as well as by providing a much-reduced settling time. Therefore, the supply current is not highly affected by DC-link voltage variation after using the optimized anti-windup PI controller.

(a)

(b)
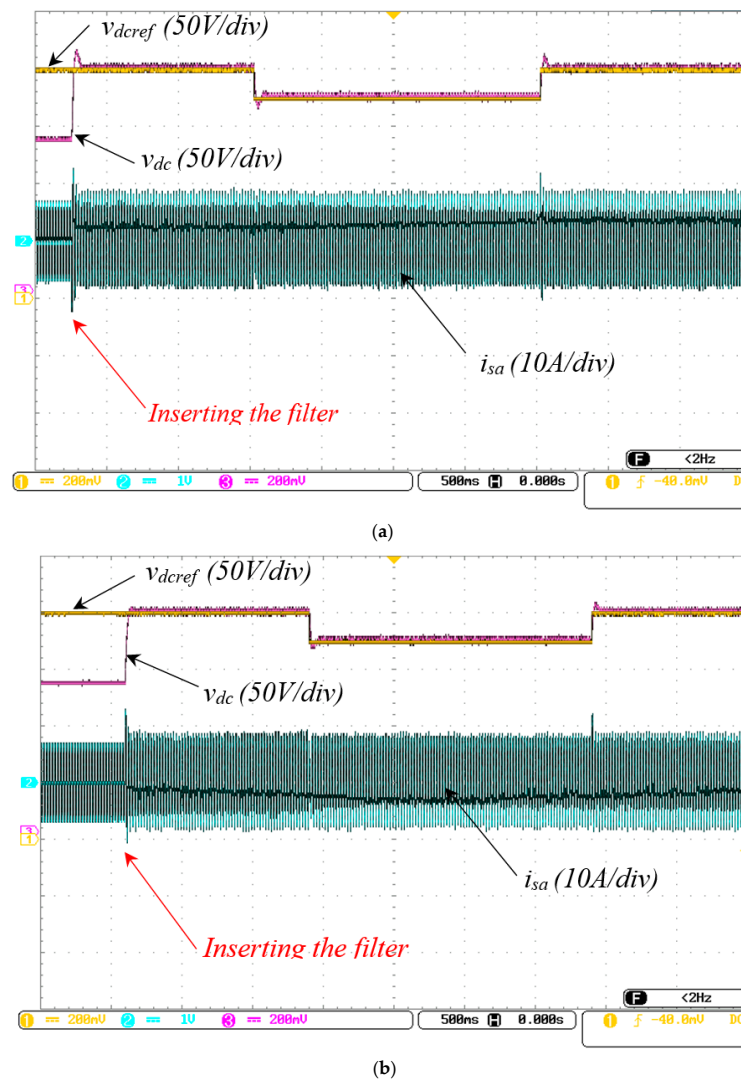
Figure 9. Response of DC bus voltage under double step change of reference voltage based on conventional (**a**) and optimized (**b**) anti-windup PI controller.

The feasibility and efficiency of the proposed control scheme have been evaluated based on power quality enhancement. Various tests have been established before connecting the PV system, comparing it with those obtained using conventional DPC such as steady-state operation, Connection/disconnection of SAPF and Load variation.

- Steady state operation

The steady state performance of both control strategies can be evaluated in Figures 10–12. The source current has been analyzed using a Fast Fourier Transformation tool (FFT). Figure 10 shows the source current and its spectrum analysis before connecting the filter (inverter), which is the same current of the load. The current has a non-sinusoidal waveform with high harmonic distortion, as shown in the spectrum graph.

The filtered current waveform when using the conventional DPC strategy is shown in Figure 11a. It was observed that the fifth and the seventh harmonic components appear in the spectrum graph in addition to the fundamental component. However, the obtained current after filtering has a sinusoidal waveform, and the higher order harmonic components are effectively suppressed when MPPC-SVM is used, which demonstrates the superiority of the proposed algorithm in harmonic current filtering.

Figure 12 illustrates the supply voltage, supply current, filter current, and the DC bus voltage. It is clearly observed that supply current has a smooth sinusoidal waveform which is in phase with the corresponding source voltage. The DC bus voltage is perfectly regulated at 160 V, whereas the inverter injects the current harmonic components needed for the main current filtering. As can be seen, good electrical signal waveforms are given after using the proposed control strategy with low distortion of the supply current.

- Disconnection/connection of SAPF

Figure 13 represents, from top to bottom: source voltage and source current, filter current, and DC bus voltage. As can be seen, before connecting the filter, the load current is totally supplied by the utility grid; as a result, the source voltage is affected by harmonic components in the supply current. The DC side capacitor is charged via the open loop scheme (through antiparallel diodes) to reach a line voltage level v_{dc} = 100 V.
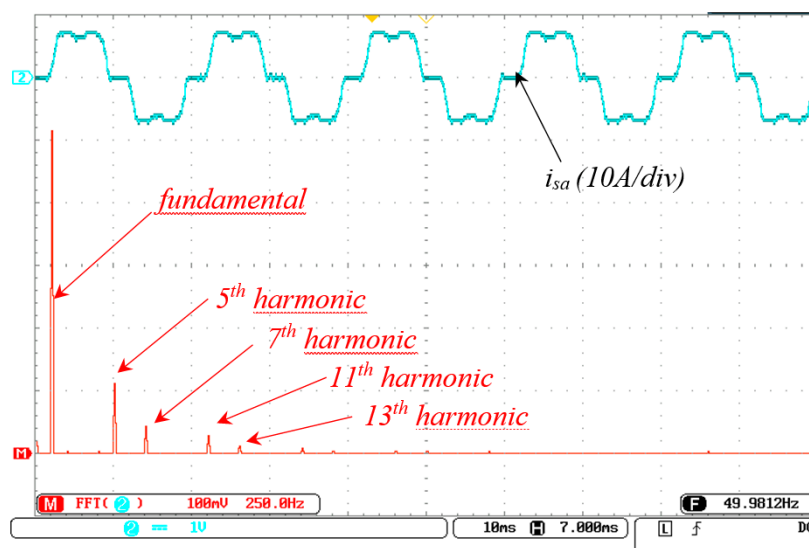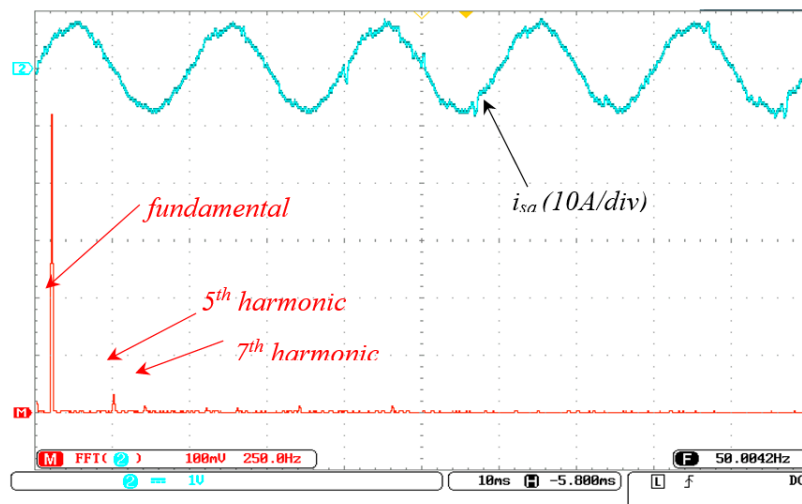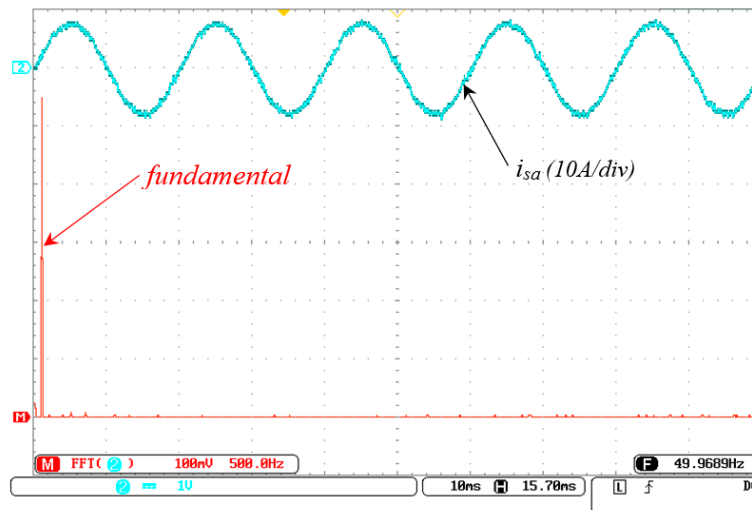

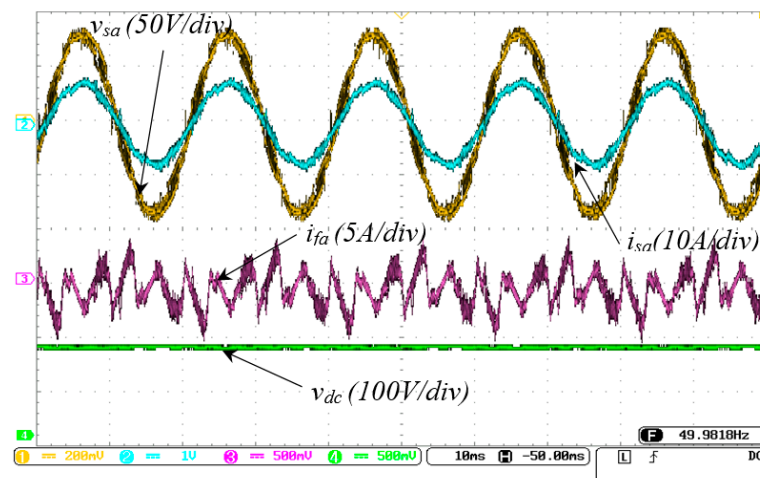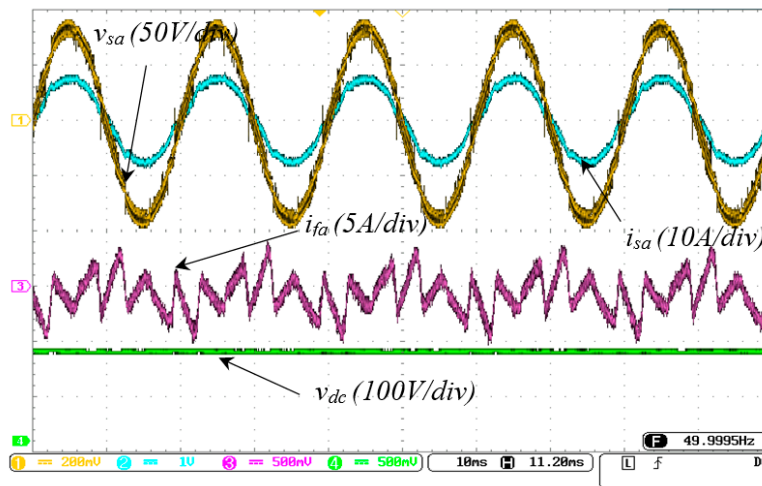**Figure 10.** FFT analysis of supply current before connecting the filter.

(**a**)

(**b**)

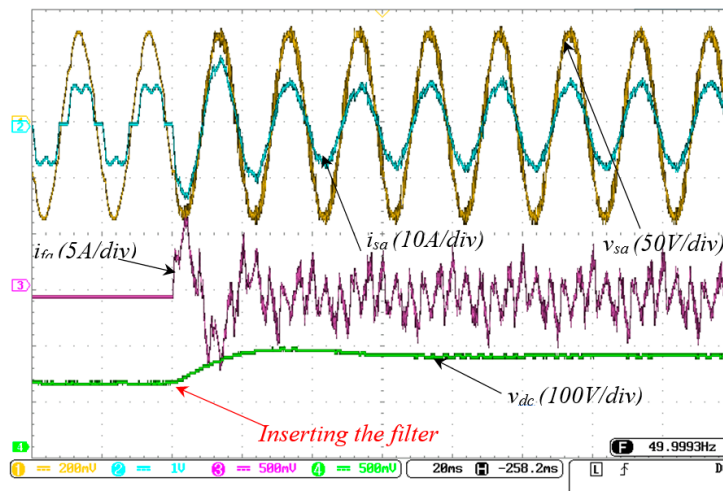**Figure 11.** FFT analysis of supply current after using conventional DPC (**a**) and MPPC-SVM (**b**) strategy.

(**a**)
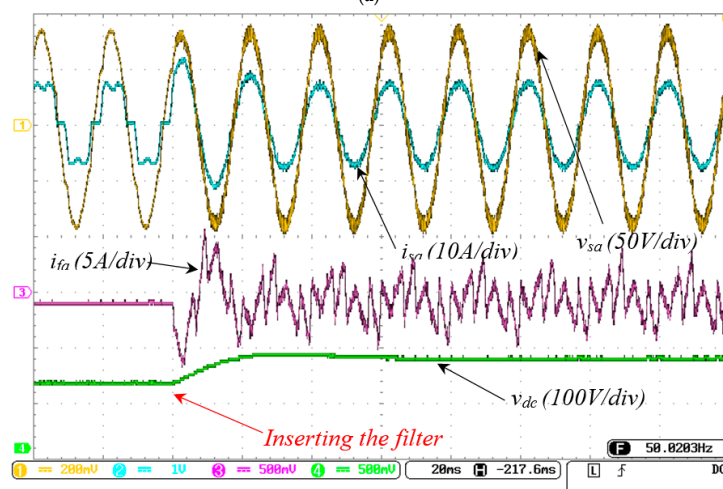
Figure 12. *Cont.*

(**b**)

Figure 12. Main parameters of the system in steady state operation after using DPC (**a**) and MPPC-SVM (**b**).


(**a**)

(**b**)

Figure 13. Main parameters of the system at filter insertion by using conventional DPC (**a**) and MPPC-SVM (**b**).

After inserting SAPF, the inverter starts to inject the current i_f that is necessary to make the supply current free from harmonics. The PSO-PI controller only needs 0.08 s to keep the DC bus voltage at its reference value 160 V. The active and reactive powers of the source are illustrated with their references in Figure 14. The reactive power is successfully compensated after connecting the filter in the case of the proposed control strategy. Hence, the active power perfectly tracked its reference with reduced ripple compared to that of a conventional DPC.


(a)

(b)
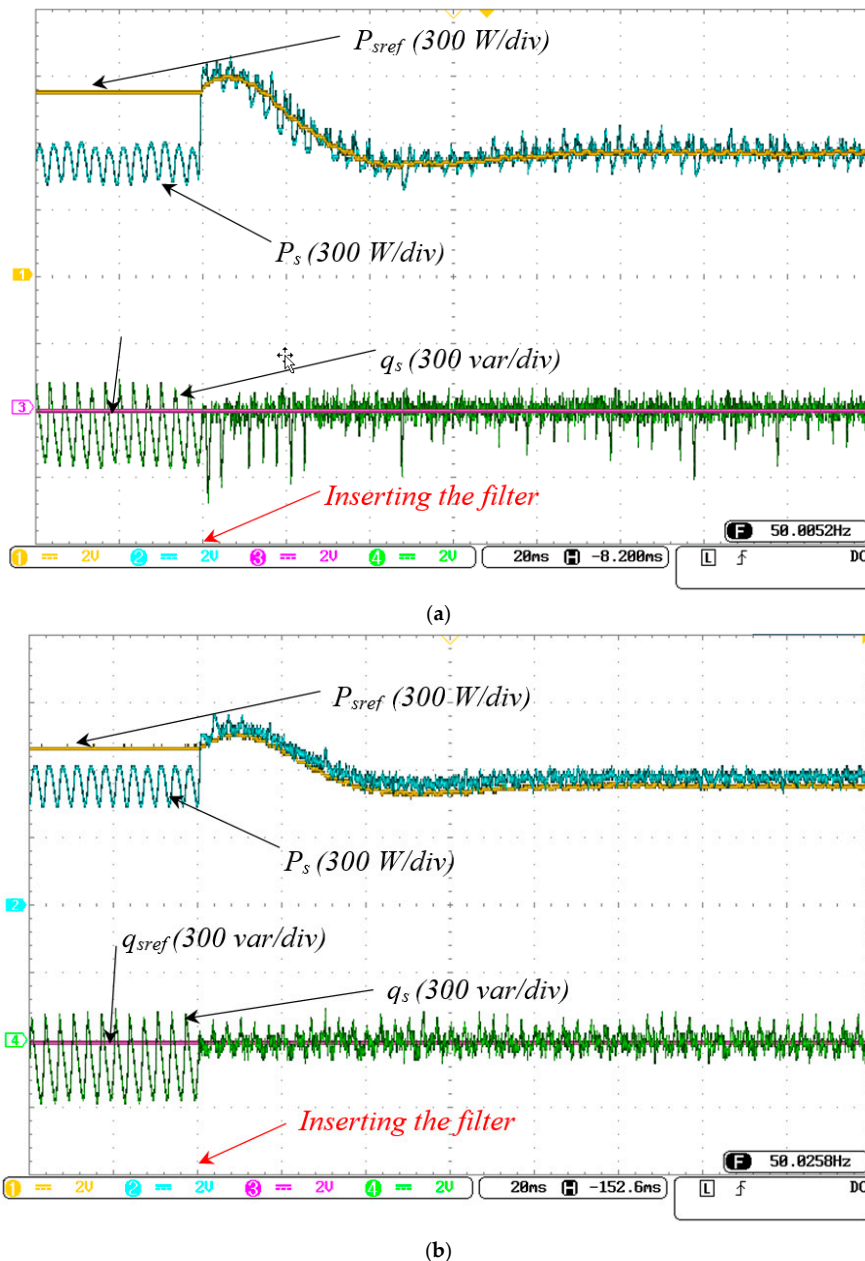
Figure 14. Active and reactive powers of the main source at filter insertion by using conventional DPC (**a**) and MPPC-SVM (**b**).

- Load variation

To demonstrate the higher effectiveness of the DC bus voltage controller, double step change in nonlinear load was established; the value of the nonlinear load presents a variation of 32% (R1= 16 Ω to R2 =11 Ω and vice versa). Very satisfactory results are achieved, as can be observed in Figure 15. It

shows a good transient behavior of the system other than smooth variation in supply current. The increase in source current leads to a slight voltage dip in the DC link capacitor voltage. During this phase, the load consumes additional energy from the capacitor to reach its need. Alternatively, an excess in DC bus voltage is seen once the supply current is decreased. However, the PSO-PI controller quickly corrects these voltage variations. Generally, the obtained results in different phases prove the superiority of the proposed control strategy in terms of power quality. It presents a better current waveform with less harmonic components, reduced active power ripples, and better reactive power compensation.
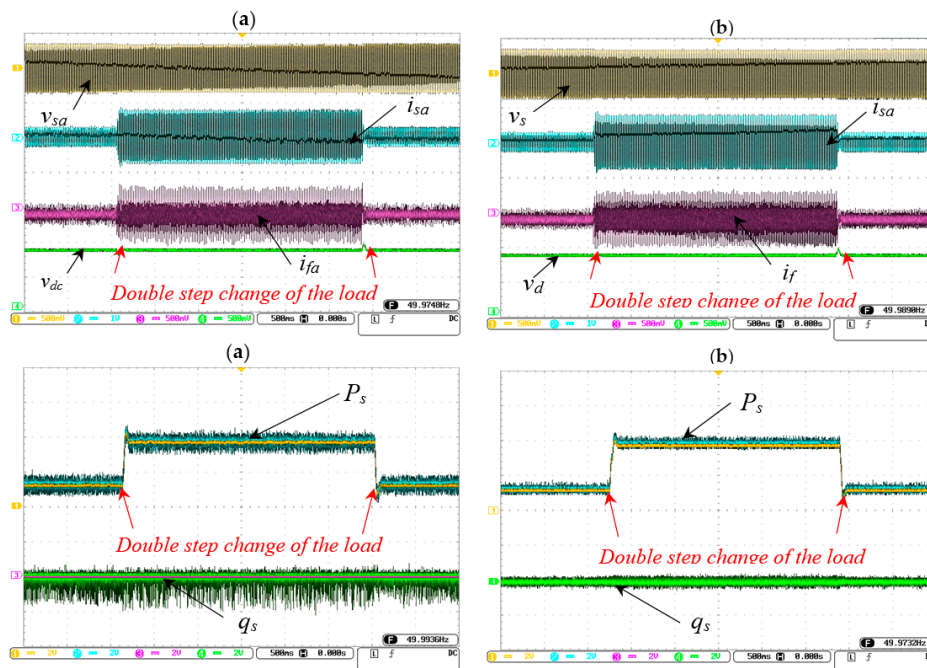
Figure 15. Main parameters of the system during load variation by using conventional DPC (**a**) and MPPC-SVM (**b**).

- SM-MPPT under variable illumination.

To demonstrate the efficiency and the robustness of SM-MPPT algorithm, a simulation test has been established under variable illumination in standalone mode. The photovoltaic generator is composed of four PV panels of 85 W associated in series. The output power of the PV generator using sliding mode MPPT-based PSO is compared to that obtained using a conventional P_O algorithm. As seen in the curves of Figure 16, sliding mode MPPT optimized by PSO perfectly follows the theoretical reference. It follows the maximum power with a very good stability and lower oscillation. However, the panels are still at their optimal power despite the sudden variation of illumination. In addition, the proposed MPPT reaches the MPP with a very short convergence time when compared to the P_O algorithm.

- Inserting the PV system.

The proposed system was designed to operate as shunt active power filter (SAPF) when the PV system is disconnected (lack of illumination); it performs power quality improvements by reducing the current harmonics of the source and enhancing its power factor, but once the PV system is connected (exist of illumination), additional active power is injected into the load/grid as can be seen in Figure 17. After connecting the PV system, in Figure 18, it is observed that the current provided by the main source is reduced, the injected current is increased, and the PV power is different to zero, whereas the active power provided by the source is reduced. The experimental tests were done in real time under

the following conditions (T = 37 °C and G = 860 W/m^2). In this test, the fixed tilt ground-mounted PV string provides its maximum available power (240 W) to the load, and the grid ensures the remaining needed power.
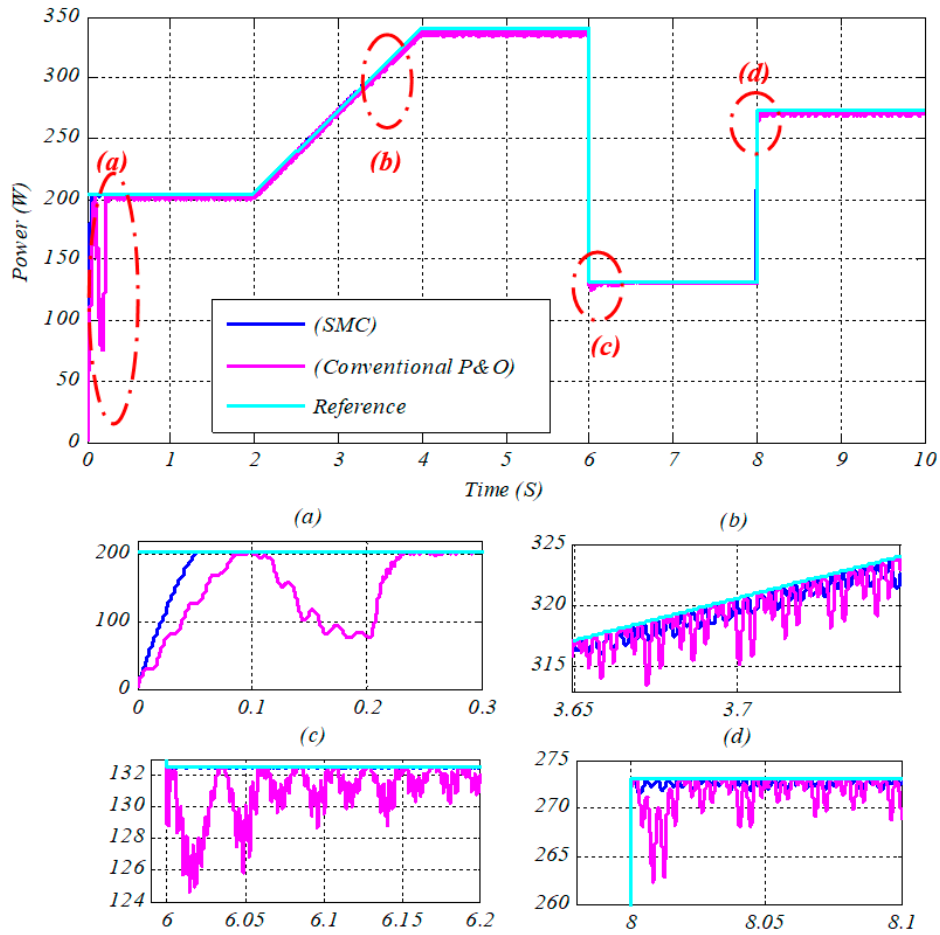

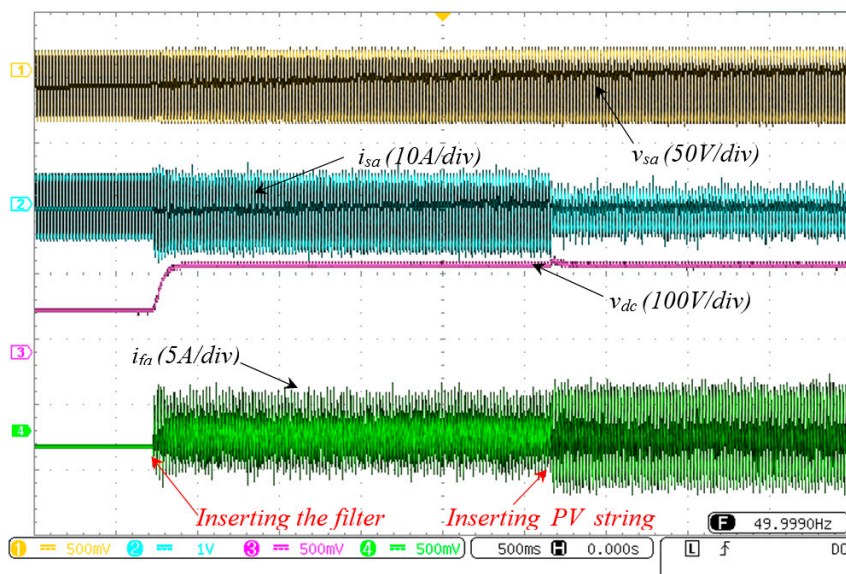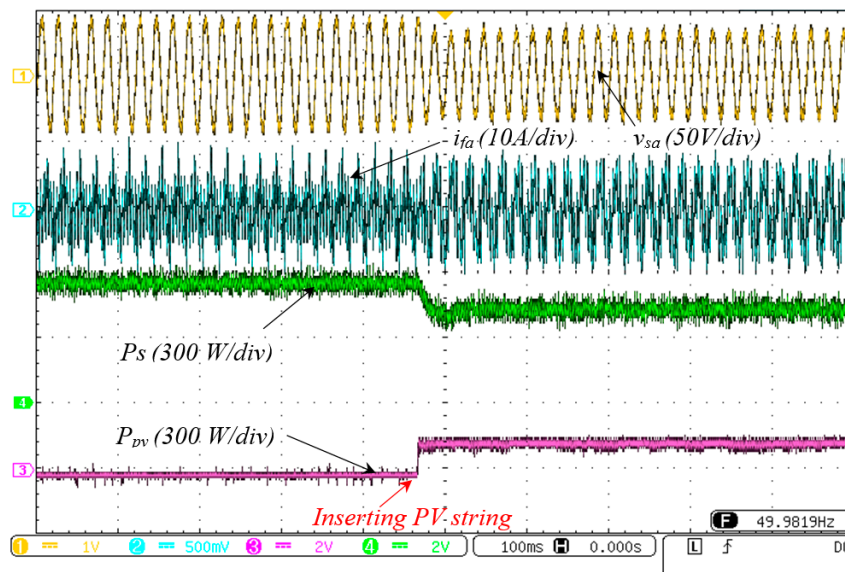**Figure 16.** Output PV Power waveform under variable illumination.

Figure 17. Obtained results in different scenarios.

Figure 18. Voltage, current, active power of the main source and PV string at PV system switch ON.

The investigated scenarios of the proposed system operation are summarized in Figure 17. It shows the results in three different phases; before connecting the inverter (filter) into the grid, after connecting the inverter into the grid (filtering phase), during the operation of the PV system. Before connecting the filter, the load was supplied directly by the source that offers the needed active and reactive power simultaneously and the harmonic currents. Once the filter is connected, the inverter provides the needed reactive power and the harmonic currents to the load in order to make the source operate with unity power factor and suppress the higher order harmonic components. Then, after connecting the PV system, the inverter performs three main functions: reactive power compensation, active power injection by PV system, and source current filtering. The three operation phases are clearly demonstrated by the source and injected current waveform, DC bus voltage, in addition to active and reactive power waveform.

It is shown in Figure 19 that the injected current after connecting PV system has a different waveform compared to that obtained in the absence of PV system, because it includes harmonic current, reactive current, and active current provided by PV panels. However, the active current does not exist before connecting PV system.

Figure 20 shows the spectrum analysis of the main source current when the PV system is connected. It is clearly shown that higher order harmonics are effectively suppressed and only the 5th and 13th harmonics appear in the spectrum graph with small magnitudes, which proves the proficiency of the proposed system in suppressing harmonic currents in addition to PV power injection.
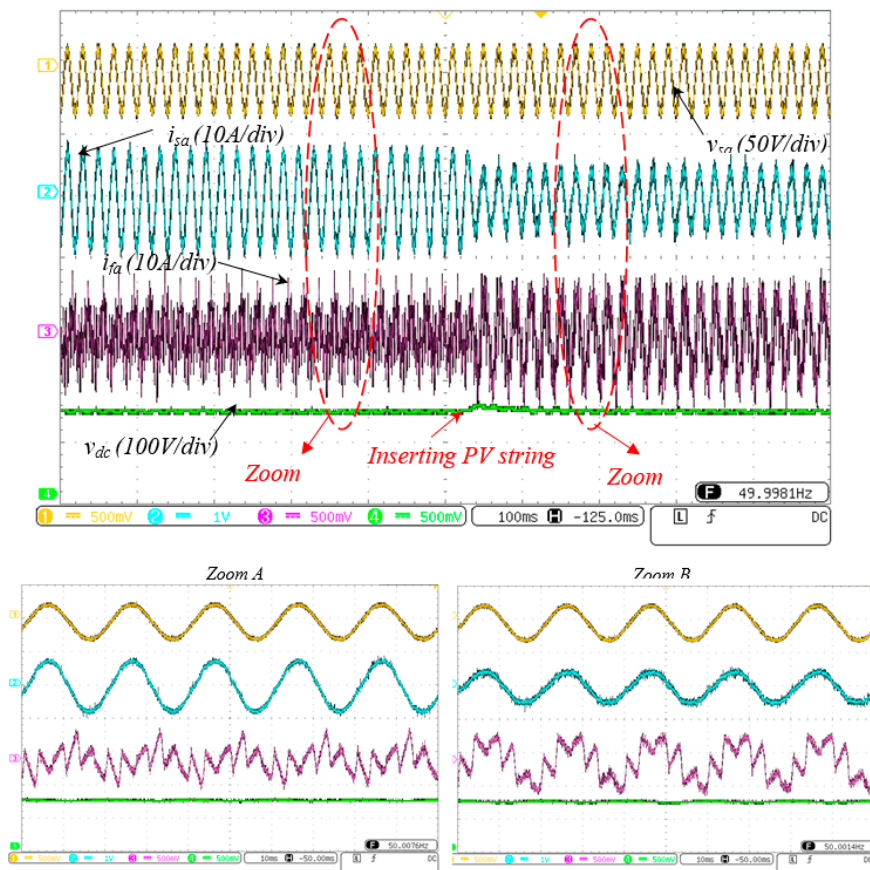
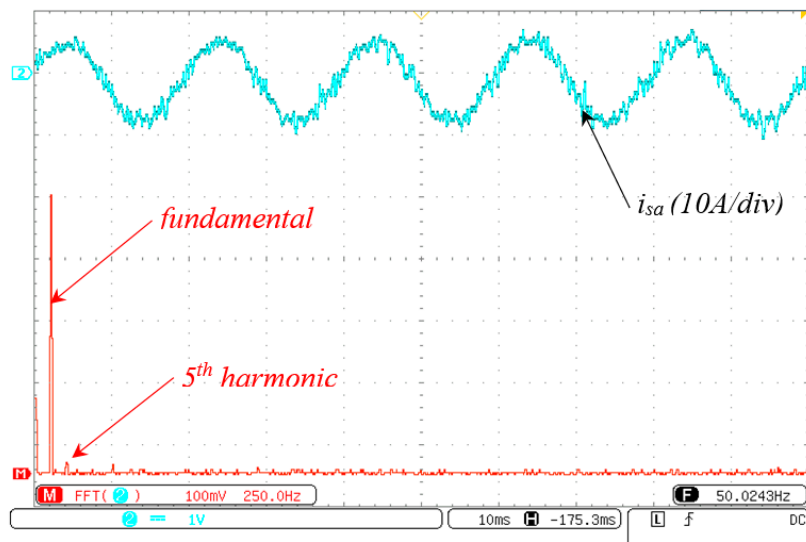**Figure 19.** Voltage, current, active power of the main source and PV string at PV system switch ON.

Figure 20. FFT analysis for supply current after connecting PV system.

7. Conclusions

In this paper, an MPC with SVM for double function grid-tied PV system has been designed and validated in an experimental prototype. The proposed control scheme replaces the cost function block of the MPC approach by SVM to operate at fixed and low switching frequencies, enhance the performance of the system, and to ensure the reliability of its hardware components. One important feature that characterizes this control strategy is the simplicity of implementation; it does not need the

coordinate transformation of system variables into rotating reference frame (d–q) as well as current control loops. In addition, it does not require a current harmonic extraction stage, which reduces the number of required sensors and minimizes the cost and the size of SAPF. Likewise, it decreases the computing time and improves accuracy. Furthermore, the voltage control vectors are calculated without using linear controllers. The efficiency of the developed SM-MPPT-based PSO algorithm has been clearly demonstrated during a sudden change in illumination. Then again, the PSO algorithm demonstrates its capability to design an optimal anti-windup PI controller that can improve the control of DC side of the inverter. The obtained results in different operating conditions demonstrate the efficiency of the proposed control scheme in terms of harmonic current filtering, power factor correction, and DC bus voltage regulation, as well as PV power injection. It offers a superior performance and higher power quality compared to conventional DPC strategies.

Author Contributions: K.A. established the major part of the present work which comprises modeling, simulation, experimental validation and analyses of the obtained results. Moreover, K.A. was mainly responsible for preparing the manuscript as well. Z.L. and B.M. contributed in simulation. Z.L. and B.R. contributed immensely in experimental validation and S.S.R. has earnestly contributed to verifying the work and finalizing the paper.

Conflicts of Interest: The authors declare no conflict of interest.

Nomenclature

v_a, v_b, v_c	Source voltage of phase a, b, c respectively (V)
v_{sa}, v_{sb}, v_{sc}	Voltage at the point of common coupling of phase a, b, c respectively (V)
i_{sa}, i_{sb}, i_{sc}	Current at the point of common coupling of phase a, b, c respectively (A)
i_{fa}, i_{fb}, i_{fc}	Filter current of phase *a*, *b*, *c* respectively (A)
i_{la}, i_{lb}, i_{lc}	Load current of phase *a*, *b*, *c* respectively (A)
R_s, R_l, R_f	Source, series load and filter resistance (Ω)
L_s, L_l, L_f	Source, series load and filter inductance (H)
R	Load resistance (Ω)
v_{dc}	DC bus voltage (V)
c_1	DC bus capacitor (F)
c_2	Capacitor at the output of the boost (F)
u_f	Voltage at output of the inverter (V)
p_s, p_{sref}	Actual and reference of active power (W)
$i_{fundamental}$	Fundamental component of the current (A)
$i_{harmonic}$	Harmonic components of the current (A)
T_s	Sampling time (S)
ε_p	Error of active power (W)
ε_q	Error of reactive power (var)
k_p, k_i	Proportional and integral gains
G_a	Anti-windup gain
P_{pv}, P_{pvref}	Measured and reference value of PV power (W)
I_{pv}	Output current of PV string (A)
u	Output of sliding mode controller
S	Sliding mode surface
K	Sliding mode gain
e	Error of DC bus voltage control loop (V)
e_{pv}	Error between the measured PV power and its reference (W)

L	Inductance of the boost (H)
THD_{i_s}	Total harmonic distortion of source current
P	Laplace operator
G	Solar irradiance (W/m^2)
T	Temperature at operating condition (C$^\circ$)
$I_{t\max}$	Maximum number of iteration

References

1. Bhim, S.; Shailendra, K.; Chinmay, J. Damped-SOGI Based Control Algorithm For Solar PV Power Generating System. *IEEE Trans. Ind. Appl.* **2017**, *53*, 1780–1788. [CrossRef]

2. Guo, Y.; Cha, J.; Liu, W.; Tian, Y. A system modeling method for optimization of a single axis solar tracker. In Proceedings of the 2010 International Conference on Computer Application and System Modeling (ICCASM), Taiyuan, China, 22–24 October 2010; Volume 11, pp. 30–34. [CrossRef]

3. Babu, B.C.; Gurjar, S. A novel simplified two-diode model of photovoltaic (PV) module. *IEEE J. Photovolt.* **2014**, *4*, 1156–1161. [CrossRef]

4. Bouzelata, Y.; Kurt, E.; Altin, N.; Chenni, R. Design and simulation of a solar supplied multifunctional active power filter and a comparative study on the current-detection algorithms. *Renew. Sustain. Energy Rev.* **2015**, *43*, 1114–1126. [CrossRef]

5. Djerioui, A.; Aliouane, K.; Bouchafaa, F. Sliding mode observer of a power quality in grid connected renewable energy systems. *Int. J. Renew. Energy Res.* **2012**, *2*, 541–548.

6. Liu, L.; Meng, X.; Liu, C. A review of maximum power point tracking methods of PV power system at uniform and partial shading. *Renew. Sustain. Energy Rev.* **2016**, *53*, 1500–1507. [CrossRef]

7. Molina, M.G.; Espejo, E.J. Modeling and simulation of grid-connected photovoltaic energy conversion systems. *Int. J. Hydrog. Energy* **2014**, *39*, 8702–8707. [CrossRef]

8. Spertino, F.; Corona, F. Monitoring and checking of performance in photovoltaic plants: A tool for design, installation and maintenance of grid-connected systems. *Renew. Energy* **2013**, *60*, 722–732. [CrossRef]

9. Rahmani-Andebili, M.; Haiying, S. Price-Controlled Energy Management of Smart Homes for Maximizing Profit of a GENCO. *IEEE Trans. Syst. Man Cybern.* **2017**, 1–13. [CrossRef]

10. Tian, H.; Mancilla-David, F.; Ellis, K.; Muljadi, E.; Jenkins, P. A cell-to-module-to-array detailed model for photovoltaic panels. *Sol. Energy* **2012**, *86*, 2695–2706. [CrossRef]

11. Laib, A.; Krim, F.; Talbi, B.; Kihal, A.; Feroura, H. Improved control of three phase dual-stage grid-connected PV system based on a predictive control strategy. *Control Eng. Appl. Inform.* **2018**, *20*, 12–23.

12. Piegari, L.; Rizzo, R.; Spina, I.; Tricoli, P. Optimized adaptive perturb and observe maximum power point tracking control for photovoltaic generation. *Energies* **2015**, *8*, 3418–3436. [CrossRef]

13. Safari, A.; Mekhilef, S. Simulation and hardware implementation of incremental conductance MPPT with direct control method using cuk converter. *IEEE Trans. Ind. Electron.* **2011**, *58*, 1154–1161. [CrossRef]

14. Algarín, C.R.; Giraldo, J.T.; Álvarez, O.R. Fuzzy logic based MPPT controller for a PV system. *Energies* **2017**, *10*, 2036. [CrossRef]

15. Ben Salah, C.; Ouali, M. Comparison of fuzzy logic and neural network in maximum power point tracker for PV systems. *Electr. Power Syst. Res.* **2011**, *81*, 43–50. [CrossRef]

16. Priyadarshi, N.; Padmanaban, S.; Mihet-Popa, L.; Blaabjerg, F.; Azam, F. Maximum power point tracking for brushless DC motor-driven photovoltaic pumping systems using a hybrid ANFIS-FLOWER pollination optimization algorithm. *Energies* **2018**, *11*, 1067. [CrossRef]

17. Messai, A.; Mellit, A.; Guessoum, A.; Kalogirou, S.A. Maximum power point tracking using a GA optimized fuzzy logic controller and its FPGA implementation. *Sol. Energy* **2011**, *85*, 265–277. [CrossRef]

18. Mohanty, S.; Subudhi, B.; Ray, P.K. A Grey Wolf-Assisted Perturb & Observe MPPT Algorithm for a PV System. *IEEE Trans. Energy Convers.* **2017**, *32*, 340–347. [CrossRef]

19. Du, Y.; Yan, K.; Ren, Z.; Xiao, W. Designing Localized MPPT for PV Systems Using Fuzzy-Weighted Extreme Learning Machine. *Energies* **2018**, *11*, 2615. [CrossRef]

20. Levron, Y.; Shmilovitz, D.; Yoash Levron, D.S. Maximum Power Point Tracking Employing Sliding Mode Control. *IEEE Trans. Circuits Syst. I Regul. Pap.* **2013**, *60*, 724–732. [CrossRef]

21. Menadi, A.; Abdeddaim, S.; Betka, A.; Benchouia, M.T. Real Time Implementation of A Fuzzy Logic Based Mppt Controller for Grid Connected Photovoltaic System. *Int. J. Renew. Energy Res.* **2015**, *5*, 236–244.

22. Mellit, A.; Kalogirou, S.A. Artificial intelligence techniques for photovoltaic applications: A review. *Prog. Energy Combust. Sci.* **2008**, *34*, 574–632. [CrossRef]

23. Antoniewicz, K.; Jasinski, M.; Kazmierkowski, M.P.; Malinowski, M. Model Predictive Control for Three-Level Four-Leg Flying Capacitor Converter Operating as Shunt Active Power Filter. *IEEE Trans. Ind. Electron.* **2016**, *63*, 5255–5262. [CrossRef]

24. Krama, A.; Laid, Z.; Boualaga, R. Anti-Windup Proportional Integral Strategy for Shunt Active Power Filter Interfaced by Photovoltaic System using Technique of Direct Power Control. *Rev. Roum. Sci. Tech. Électrotech. Énerg.* **2017**, *62*, 252–257.

25. Emadi, A.; Abdolhosein, N.; Bekiarov, S. *Uninterruptible Power Supplies and Active Filters*; CRC Press: Boca Raton, FL, USA, 2005; ISBN 0849330351.

26. Musa, S.; Radzi, M.A.M.; Hizam, H.; Wahab, N.I.A.; Hoon, Y.; Zainuri, M.A.A.M. Modified synchronous reference frame based shunt active power filter with fuzzy logic control pulse width modulation inverter. *Energies* **2017**, *10*, 758. [CrossRef]

27. Bouzidi, M.; Benaissa, A.; Barkat, S. Hybrid direct power/current control using feedback linearization of three-level four-leg voltage source shunt active power filter. *Int. J. Electr. Power Energy Syst.* **2014**, *61*, 629–646. [CrossRef]

28. Roasto, I.; Romero-cadavai, E.; Martins, J.; Smolenski, R. State of the Art of Active Power Electronic Transformers for Smart Grids. In Proceedings of the IECON 2012—38th Annual Conference on IEEE Industrial Electronics Society, Montreal, QC, Canada, 25–28 October 2012; pp. 5241–5246.

29. Boukezata, B.; Gaubert, J.P.; Chaoui, A.; Hachemi, M. Predictive current control in multifunctional grid connected inverter interfaced by PV system. *Sol. Energy* **2016**, *139*, 130–141. [CrossRef]

30. Benaissa, A.; Rabhi, B.; Benkhoris, M.F.; Zellouma, L. An investigation on combined operation of five-level shunt active power filter with PEM fuel cell. *Electr. Eng.* **2017**, *99*, 649–663. [CrossRef]

31. Hoon, Y.; Radzi, M.A.M.; Hassan, M.K.; Mailah, N.F. Control algorithms of shunt active power filter for harmonics mitigation: A review. *Energies* **2017**, *10*, 2038. [CrossRef]

32. Jayanand, B. Harmonic and Reactive Power Compensation of Grid Connected Photovoltaic System. *Procedia Technol.* **2015**, *21*, 438–442. [CrossRef]

33. Saad, S.; Zellouma, L. Fuzzy Logic Controller for Three-phase Shunt Active Filter Compensating Harmonics and Reactive Power Simultaneously. *Electr. Power Syst. Res.* **2009**, *79*, 1337–1341. [CrossRef]

34. Benchouia, M.T.; Ghadbane, I.; Golea, A.; Srairi, K.; Benbouzid, M.E.H. Implementation of adaptive fuzzy logic and PI controllers to regulate the DC bus voltage of shunt active power filter. *Appl. Soft Comput. J.* **2015**, *28*, 125–131. [CrossRef]

35. Chaoui, A.; Gaubert, J.-P.; Krim, F. Power quality improvement using DPC controlled three-phase shunt active filter. *Electr. Power Syst. Res.* **2010**, *80*, 657–666. [CrossRef]

36. Krama, A.; Zellouma, L.; Rabhi, B. Improved control of shunt active power filter connected to a photovoltaic system using technique of direct power control. In Proceedings of the 2016 8th International Conference on Modelling, Identification and Control, ICMIC 2016, Algiers, Algeria, 15–17 November 2016.

37. Ouchen, S.; Betka, A.; Abdeddaim, S.; Menadi, A. Fuzzy-predictive direct power control implementation of a grid connected photovoltaic system, associated with an active power filter. *Energy Convers. Manag.* **2016**, *122*, 515–525. [CrossRef]

38. Bouafia, A.; Gaubert, J.-P.; Krim, F. Predictive Direct Power Control of Three-Phase Pulsewidth Modulation (PWM) Rectifier Using Space-Vector Modulation (SVM). *IEEE Trans. Power Electron.* **2010**, *25*, 228–236. [CrossRef]

39. Malinowski, M.; Jasinski, M.; Kazmierkowski, M.P. Simple Direct Power Control of Three-Phase PWM Rectifier Using Space Vector Modulation. *EPE J.* **2003**, *13*, 28–34. [CrossRef]

40. Tarisciotti, L.; Formentini, A.; Gaeta, A.; Degano, M.; Zanchetta, P.; Rabbeni, R.; Pucci, M. Model Predictive control for Shunt Active Filters with Fixed Switching Frequency. *IEEE Trans. Ind. Appl.* **2016**. [CrossRef]

41. Abu-rub, H.; Member, S.; Holtz, J.; Rodriguez, J.; Member, S.; Baoming, G. Medium-Voltage Multilevel Converters—State of the Industrial Applications. *IEEE Trans. Ind. Electron.* **2010**, *57*, 2581–2596. [CrossRef]

42. Abido, M.A. Optimal design of power-system stabilizers using particle swarm optimization. *IEEE Trans. Energy Convers.* **2002**, *17*, 406–413. [CrossRef]

43. Pati, S.; Sahu, B.K.; Panda, S. Hybrid differential evolution particle swarm optimisation optimised fuzzy proportional–integral derivative controller for automatic generation control of interconnected power system. *IET Gener. Transm. Distrib.* **2014**, *8*, 1789–1800. [CrossRef]

44. Eberhart, R.; Kennedy, J. A new optimizer using particle swarm theory. In Proceedings of the Sixth International Symposium on Micro Machine and Human Science, Nagoya, Japan, 4–6 October 1995; pp. 39–43. [CrossRef]

45. Benhabib, M.C.; Saadate, S. A new robust experimentally validated Phase-Looked Loop for power electronic control. *EPE J.* **2005**, *15*, 36–48. [CrossRef]

46. Rodriguez, J.; Cortés, P. *Predictive Control of Power Converters and Electrical Drives*; John Wiley & Sons: Hoboken, NJ, USA, 2012; ISBN 9781119963981.

47. Karatepe, E.; Boztepe, M.; Colak, M. Neural network based solar cell model. *Energy Convers. Manag.* **2006**, *47*, 1159–1178. [CrossRef]

48. Bhuvaneswari, G.; Annamalai, R. Development of a solar cell model in MATLAB for PV based generation system. In Proceedings of the 2011 Annual IEEE India Conference, Hyderabad, India, 16–18 December 2011. [CrossRef]

49. Villalva, M.G.; Gazoli, J.R.; Filho, E.R. Comprehensive Approach to Modeling and Simulation of Photovoltaic Arrays. *IEEE Trans. Power Electron.* **2009**, *24*, 1198–1208. [CrossRef]

50. Saadi, A.; Becherif, M.; Ramadan, H.S. Hydrogen production horizon using solar energy in Biskra, Algeria. *Int. J. Hydrog. Energy* **2016**, *41*, 21899–21912. [CrossRef]

51. Castillo-Toledo, B.; Castro-Linares, R. On robust regulation via sliding mode for nonlinear systems. *Syst. Control Lett.* **1995**, *24*, 361–371. [CrossRef]

52. Zellouma, L.; Rabhi, B.; Krama, A.; Benaissa, A.; Benkhoris, M.F. Simulation and real time implementation of three phase four wire shunt active power filter based on sliding mode controller. *Rev. Roum. Des. Sci. Tech. Ser. Electrotech. Energ.* **2018**, *63*, 77–82.

53. Vandenbergh, F.; Engelbrecht, A.P. A Cooperative Approach to Particle Swarm Optimization. *IEEE Trans. Evol. Comput.* **2004**, *8*, 225–239. [CrossRef]

54. Sun, J.; Lai, C.; Wu, X. *Particle Swarm Optimization: Classical and Quantum Perspectives*; CRC Press: Boca Raton, FL, USA, 2012; ISBN 13: 978-1-4398-3577-7.

55. Shi, Y.; Eberhart, R. A modified particle swarm optimizer. In Proceedings of the 1998 IEEE International Conference on Evolutionary Computation Proceedings and IEEE World Congress on Computational Intelligence (Cat. No. 98TH8360), Anchorage, AK, USA, 4–9 May 1998; pp. 69–73. [CrossRef]

56. Lee, H.; Lee, J. Design of iterative sliding mode observer for sensorless PMSM control. *IEEE Trans. Control Syst. Technol.* **2013**, *21*, 1394–1399. [CrossRef]